Interfacial rheology of model water-air microgels laden interfaces: effect of cross-linking

Marie-Charlotte Tatry, Eric Laurichesse, Jan Vermant, Valérie Ravaine, Véronique Schmitt

Interfacial rheology of model water-air microgels laden interfaces: effect of cross-linking.

Marie-Charlotte Tatry[1,2], Eric Laurichesse[1], Jan Vermant[3], Valérie Ravaine[2*], Véronique Schmitt[1*]

[1] Centre de Recherche Paul Pascal (CRPP), UMR 5031, Univ. Bordeaux, CNRS, 115 Avenue du Dr Albert Schweitzer, 33600 Pessac, FRANCE
[2] Univ. Bordeaux, CNRS, Bordeaux INP, ISM, UMR 5255, 33400 Talence, FRANCE
[3] Laboratory of Soft Materials, Department of Materials, ETH Zürich, Vladimir-Prelog-Weg 5, CH-8093, Zurich, SWITZERLAND

mariecharlottetatry@wanadoo.fr, eric.laurichesse@crpp.cnrs.fr, jan.vermant@mat.ethz.ch,

* co-corresponding authors vravaine@enscbp.fr (+33 5 56 84 66 13), veronique.schmitt@crpp.cnrs.fr (+33 5 56 84 56 67)

Abstract

Hypothesis The mechanical properties of model air/water interfaces covered by poly(N-isopropylacrylamide) microgels depend on the microgels deformability or in other words on the amount of cross-linker added during synthesis.

Experiments The study is carried out by measuring the apparent dilational, the compression and the shear moduli using three complementary methods: 1) the pendant drop method with perturbative areas, 2) the Langmuir trough compression, and 3) shear rheology using a double wall ring cell mounted onto a Langmuir through.

Findings In the range of surface coverages studied, the interfaces exhibit a solid-like behavior and elasticity goes through a maximum as a function of the surface pressure. This is observable whatever the investigation method. This maximum elasticity depends on the microgel deformability: the softer the microgels the higher the value of the moduli. The mechanical behavior of model interfaces is discussed, taking into account the core-shell structure of the particles and their packing at the interface.

Keywords: microgels, particle-laden interfaces, interfacial rheology, elasticity, solid-like interfacial behavior

ABBREVIATIONS

AFM: atomic force microscopy

BIS: *N,N'*-methylenebis(acrylamide)

CryoSEM: scanning electron cryomicroscopy

DLS: dynamic light scattering

DWR: double wall ring

NIPAM: *N*-isopropylacrylamide

PDMS: polydimethilsiloxane

PF-QNM: peak force nanomechanical mapping

pNIPAM: poly(*N*-isopropylacrylamide)

pNIPAM-co-MAA: poly-(*N*-isopropylacrylamide-*co*-methacrylicacid

SANS: small angle neutron scattering

SEM : scanning electron microscopy

VELD: viscoelastic linear domain

VPTT: volume phase transition temperature

I) Introduction and state of the art

Microgels are soft and deformable particles consisting of a loosely cross-linked polymer network, able to swell or contract upon application of an external stimulus. Temperature can be a tuning parameter, in the case of poly(*N*-isopropylacrylamide) (pNIPAM) microgels, which serve as a gold standard for this class of materials [1]. pNIPAM microgels adsorb spontaneously at model liquid interfaces as shown long ago by Zhang and Pelton [2]. Since this pioneering work, this feature has been confirmed and numerous works focused on the conformation of adsorbed microgels at solid [3] and liquid interfaces [4]. It has been shown, both experimentally and theoretically [5-10], that microgels spontaneously flatten at liquid interfaces and that they mainly protrude towards water [5] depending on the respective solvent quality parameters of both liquid phases [10]. Moreover, pNIPAM microgels exhibit a core-shell structure, the core being more cross-linked than the shell, due to differences in reactivity of the monomer and the crosslinker [11]. As a consequence microgels present an uneven deformation at the interface, with a characteristic "fried egg" structure [6]. The cross-linking density of microgels that governs their deformability has also been shown to influence their flattening [5,11]. The less cross-linked the microgels, the more the particles deform at the interface [6,9,10]. The evolution of the surface pressure π as a function of area A can be understood thanks to the visualization of the microgels conformation, which was achieved by SEM or AFM after compression of the microgels using Langmuir trough followed by their transfer onto a flat solid substrate [8,9,12]. It is now well understood that the π-A curve exhibits five domains [8,9,12] upon compression (see Fig. 1). The first one (domain I) where $\pi \sim 0$ corresponds to a gas of isolated non-interacting microgels or non-percolated clusters. When shells begin to interact and interpenetrate the pressure increases sharply (domain II). Then the pressure increases more smoothly or even exhibits a plateau value (domain III). In this domain, either two solid phases coexist with two

hexagonal lattice distances (for hard microgels) or one hexagonal condensed phase with a decreasing lattice parameter (soft microgels), where the shell becomes compressed [9]. For higher compressions, the cores of the microgels interact, likely trough Hertzian interactions (*i.e.* interactions between two elastic spheres in contact) as proposed in [13], until reaching their limit of compressibility (domain IV) and then the collapse leading to buckling of the interface and film breakdown may even be observed (domain V). The kinetics of adsorption at model interfaces has also been studied [14]. Microgels spontaneously adsorb above a critical concentration whose value is higher for charged microgels compared to neutral ones. Once this concentration is exceeded, the stationary interfacial tension value depends neither on the microgel concentration nor on their cross-linking density or presence of charges. It corresponds to the high surface pressure at the end of the third domain, meaning that spontaneous adsorption results in a dense surface coverage.

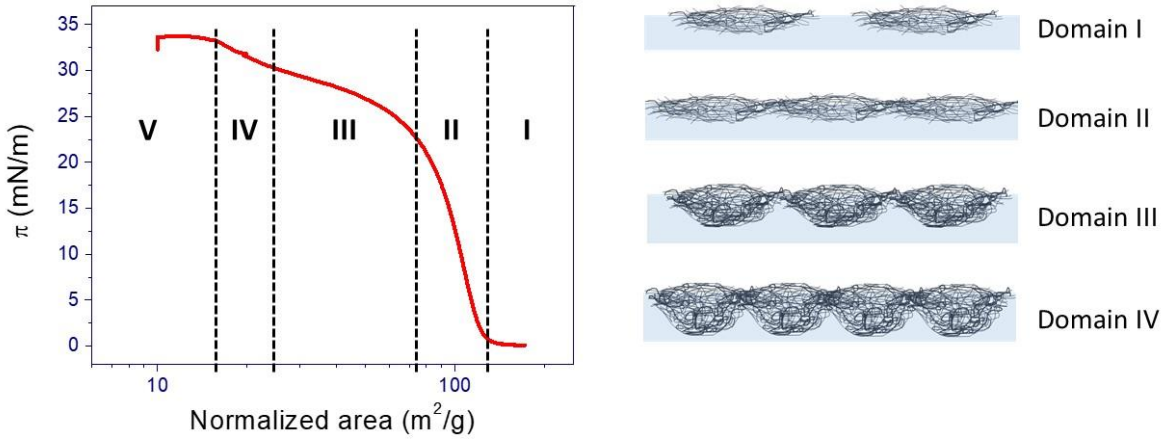

Figure 1: Surface pressure as a function of the area per microgel on an oil-water interface. Definition of the domain and schematic representation of the microgel profile in the various domains, domain V corresponding to the collapse. Adapted from [12]

Parallel to this work dedicated to model interfaces, researchers also investigated the ability of microgels to stabilize emulsions [15-23]. Owing to the responsiveness of the polymer composing microgels, the soft particles can swell or collapse upon changing the thermodynamic

parameters and therefore their ability to stabilize emulsion may also depend on these parameters [6,19,20]. Microgels exhibit peculiar properties that make them specific emulsion stabilizers with original properties, intermediate between polymeric surfactants and rigid particles [19,21]. As for hard particles, microgels adsorb quasi irreversibly, leading to very stable emulsions also called Pickering or solid-stabilized emulsions. Additionally, due to the high adsorption energy, mechanical behavior of the interface is likely a paramount parameter. Literature studies about 2D rheology for microgels-laden surfaces remain rare, the more important ones being [8,12,24-28]. Attempts to link 2D rheology to bubble or drop stability have been proposed. In 2010, Brugger and co-workers [25] conducted the first interfacial rheology experiments on poly-(*N*-isopropylacrylamide-*co*-methacrylic acid (pNIPAM-co-MAA)-laden fluid interfaces by carrying out shear and dilational rheology. Depending on pH, these microgels were charged (or non-charged respectively) and swollen with a 440 nm hydrodynamic diameter (or collapsed respectively with a 275 nm hydrodynamic diameter) at pH 9 (at pH 3 respectively). The authors showed that at pH 3, the interfacial tension is smaller, the interface coverage is higher, the linear regime is limited to smaller strains, the shear elasticity is smaller, the interface is more brittle and the emulsions are less stable than at pH 9. They concluded that the sensitivity towards shear determines the emulsion stability. From the observations of microgel packing at emulsion drop surfaces through CryoSEM, Destribats *et al.* [6] hypothesized that a higher shell interpenetration could explain a better resistance to mechanical disturbances for softer microgels compared to harder ones. In 2013, Cohin and co-workers [26] using particle tracking at the air-water interface covered by pNIPAM microgels studied the interfacial diffusion. They showed that at 10^{-2} wt% the interface is fully covered and the Brownian diffusivity is arrested. The compression elastic modulus measured by the pendant drop method was 100 times smaller than that with linear pNIPAM chains around the lower critical solubility temperature (LCST) [29]. Using the same technique, in 2014, Pinaud *et al.* [12] measured the elastic modulus during

pPNIPAM microgels adsorption onto a dodecane-water interface corresponding to various surface pressures for two cross-linking densities. They showed the existence of a maximum in elasticity (on the order of 50 mN/m for π~15 mN/m) independently of the cross-linking density. This surface pressure belonged to the second domain where microgels interact through their shells. Two years later, Rey *et al.* [8] measured the effect of smaller pNIPAM-co-MAA microgels concentration on the rheological behavior of a water-hexane interface using an interfacial microdisk rheometer with the Langmuir trough. They confirmed the existence of a maximum of viscoelasticity measured at 0.5Hz as a function of the interfacial pressure in the domain II. At low pressures, the so-called surface storage modulus G'_S increased corresponding to the compression of the shell-shell hexagonal lattice up to a value close to 1 mN/m. When the systems entered the coexistence domain, the elasticity of the interface starts to saturate as noted by the authors [8] followed by the nucleation of clusters of particles in core-core contact that relaxes the stress of the shell-shell network. When the second lattice percolated a second increase of G'_S was observed. Similar results were obtained by dilational measurements and discussed by Akentiev *et al* on pNIPAM microgels [27]. The effect of the 1 µm-sized pNIPAM-co-allylglycine microgel concentration has also been studied [28] at the PDMS-water interface by preparing Gibbs or Langmuir monolayers. At low surface coverage, passive microrheology showed that the interface mainly exhibits an elastic response, dominated by aggregated structures of microgels that formed at the interface. At high surface coverage, microgels formed densely packed monolayers. Using microsized magnetic particles as local active rheological probes, the authors observed four regimes in microgel concentration where elasticity was suggested to originate from different sources, in agreement with previous results and interpretations. When concentration increased, first the formation of aggregates leads to a viscoelastic response, the elasticity increased due to shell compression, then, a decrease of elasticity is observed which was attributed to the interfacial stress relaxation owing to folding

in the third direction and to the change from shell-shell to core-core interactions. Finally, when the distance between microgels became lower than 1 µm, the elasticity increased again through Hertzian interactions between cores. The authors also concluded that the microgel monolayers acted similarly to soft glassy materials. Recently, Yan *et al.* [30] have also shown that monolayers of shrunken pNIPAM microgels above VPTT were more easily compressed compared to monolayers consisting of swollen pNIPAM microgels.

From this brief literature review, it seems that the main points on which results converge are the dominant elastic behavior of microgels-laden interfaces and the existence of a maximum elasticity with concentration or equivalently surface pressure. However, the values of the elastic moduli at the maximum as well as the parameters tuning this maximum have not been identified yet. We wonder whether intrinsic microgel deformability is controlling interfacial mechanical properties. To test this hypothesis, we aim, herein, at characterizing the mechanical behavior of interfaces covered by microgels exhibiting variable deformability (or in other words different cross-linking densities), all other parameters remaining constant. Therefore, in the present paper, we combine various techniques to get a clearer insight into the mechanical behavior of such interfaces. To do that, we measure the dilation and compression, as well as the shear moduli using the pendant drop method with perturbative areas, the Langmuir trough compression and shear with controlled surface pressure respectively. In all cases, the interfaces exhibit solid-like behavior and the magnitude of the elastic moduli goes through a maximum as a function of the surface pressure. This maximum in elastic response depends on the microgel deformability: the softer the microgels the higher the maximal elasticity. The mechanical behavior of model interfaces is discussed taking into account the microgels core-shell structure and the microgels packing at the interface.

II) Material and methods

II.1 Chemicals

All reagents were purchased from Sigma-Aldrich. Prior to use, *N*-isopropylacrylamide (NIPAM) was recrystallized from hexane (ICS) and dried overnight under vacuum. *N,N'*-methylenebis(acrylamide) (BIS, purity 99%) and potassium persulfate (KPS, purity 99%) for the synthesis were used as received. Milli-Q water was used for all synthesis reactions, purification, and solution preparation.

II.2. Particles synthesis and purification

pNIPAM microgels with at different cross-linking compositions (1.5, 2.5 and 5 mol% respectively) were obtained as previously described [14] by an aqueous free-radical precipitation polymerization, as classically employed for the synthesis of thermo-responsive microgels and especially pNIPAM microgels (see Supporting Information SI 1). The amount of the cross-linker BIS was varied from 1.5 to 5 mol% compared to NIPAM.

The obtained suspensions were purified to remove possible synthesis residues, such as water-soluble linear polymer chains, by centrifugation-redispersion in pure water cycles (16 000 rpm = 29 000 g_T where g_T is the gravitational constant 9.81 $m.s^{-2}$ during 1 hour at 24°C). After each centrifugation, the supernatant surface tension was measured by the pendant drop method. Purification was repeated until reaching the one of pure water (72 mN/m). These purifications steps are of utmost importance because it has been shown earlier that synthesis residues exhibit themselves the ability to adsorb at interfaces [14] or to stabilize hexadecane-in-water emulsions over several months [31].

II.3 Determination of the microgel concentration

After purification, the mass of particles m_{part} (in wt%) in the suspension was determined by the drying method. At 50°C, Lele *et al.* [32] have established that the microgels are

composed of 29 wt% of polymer and 71 wt% of water. Based on this result, the number of particles can be estimated using the following relation (Eq. 1):

$$n = \frac{6m_{pol}}{\pi\left(d_H^{50°C}\right)^3}\left(\frac{0.71}{\rho_{pol}} + \frac{0.29}{\rho_{water}}\right) \quad \text{Eq. 1}$$

where $\rho_{pol} = 1.269$ g.cm^{-3} and $\rho_{water} = 1$ g.cm^{-3} are the density of polymer and water respectively, $d_{50°C}$ is the hydrodynamic diameter of the microgels at 50°C measured by dynamic light scattering (see values in Table I) and m_{part} the amount of particles determined by the dry extract at 50°C.

II.4 Particle size characterization

Microgel hydrodynamic diameters and polydispersity index were determined by dynamic light scattering (DLS) with a Zetasizer Nano S90 Malvern Instruments. The polydispersity index (PDI) is given by the cumulant analysis method. The synthesized characteristics are given in (Table 1):

Table 1: sum-up of the synthesized microgels

Sample name	NIPAM (mM)	BIS (mol%) With respect to NIPAM	$d_{25°C}$ (PDI) (nm)	$d_{50°C}$ (PDI) (nm)
pNIPAM-1.5	62	1.5	680 (0.030)	295 (0.076)
pNIPAM-2.5	62	2.5	620 (0.012)	273 (0.120)
pNIPAM-5	62	5.0	633 (0.042)	358 (0.089)

II.5 Dynamic dilational elasticity measurements with the pendant drop method

To determine the rheological properties of model air/water interfaces, covered by microgels, the pendant drop method, also called dilatational or dilational elasticity, has been used (Tracker™ Automatic Drop Tensiometer from Teclis Scientific). It consists in studying the interface mechanical response to compression-dilatation cycles. An aqueous drop of 8 µL

composed of a microgel suspension at a concentration between 0.01 wt% and 0.5 wt% was formed at the tip of a needle and wad submitted to a sinusoidal variation of its area A (Eq. 2):

$$A = A_0 \sin(2\pi f t) \quad \text{Eq. 2}$$

where f is the oscillating frequency set to 0.1 Hz and A_0 is the variation amplitude chosen small enough to belong to the linear domain. This technique of course has limitations for strongly elastic interfaces [33]. In the present case, the measured elasticity does not result from Gibbs elasticity but rather originates from interactions between adsorbed particles. As a consequence, the pressure in the drop may change more quickly and the shape may diverge from the Laplacian (i.e. that can be fitted by the Young-Laplace equation) shape [34] but this was not noticeable in the present experiment. For simplicity, we chose analyzing the drop shape, as it is frequently done in literature, keeping in mind the possible discrepancies. We therefore defined an apparent complex dilatational surface elasticity defined as:

$$E^*_{app} = \frac{d\gamma^*_{int}}{d \ln A^*} \quad \text{Eq. 3}$$

E^*_{app} is composed of a real part called apparent dilational elastic modulus E'_{app} and an imaginary part E''_{app} called apparent dilational loss modulus. A first experiment showed that E'_{app} and E''_{app} remained constant for A_0 varying from 2 to 10% of the initial drop area. The amplitude was then fixed to 5% of the initial drop area. It was checked that the Bond number, that quantifies gravitational forces and tension forces number, defined as:

$$B_0 = \frac{\rho_{water}\, g_T\, R^2}{\gamma} \quad \text{Eq. 4}$$

was larger than 0.1 ensuring a Laplacian shape of the drop. In this equation, ρ_{water} is the water phase density, R the drop radius.

As the stationary value of γ and therefore the surface pressure (defined as $\pi=\gamma_0-\gamma$ where γ_0 is the air-water pristine surface tension (72.8mN/m)) is independent of the microgel concentration [14], we had to perform the dilational viscoelastic measurements during microgel adsorption

that is to say during the evolution of γ (see Supporting Information SI 2). At a given time t, the surface tension and therefore the surface pressure is measured as well as the apparent elastic dilational modulus. The curve $E'_{app} = f(\pi)$ can therefore be plotted.

As the adsorption kinetics of microgels are unequal as a function of the cross-linking density, the microgel concentration was adapted so the half adsorption time $t_{1/2}$ is long enough (larger than 100 s) compared to the oscillation duration. It was previously checked that, for a given cross-linking density, the elastic modulus at a fixed pressure is independent of the concentration [14].

II.6. Interfacial static compression modulus

From the Langmuir compression experiments, as the surface is decreased and the two dimensional pressure is measured, the compression elastic modulus can also be estimated through Eq. 5. As the compression is not isotropic but rather uniaxial the modulus will be denoted here as E_G (rather than K).

$$E_G = -\frac{d\,\pi}{d\,\ln A} \qquad \text{(Eq. 5)}$$

Most of the Langmuir compression isotherms have been performed with a homemade Teflon trough whose size is 145 mm width and 690 mm length equipped with two mobile barriers with a protocol described in [9]. Isopropanol has been chosen as it plays the role of volatile non cosolvent [35]. Note that we checked that the obtained curve did not depend on the compression rate neither on the initial suspension concentration providing the expanded volume was adapted to deposit the same amount of microgels.

II.7. Interfacial shear rheology at controlled surface pressure

Using AFM and pendant drop method, it has been shown that the adsorbed microgel morphologies can be determined as a function of the surface pressure. However, these methods do not give access to the mechanical interface behavior at stationary state. Indeed, in the previously described pendant drop method, the surface pressure is not controlled but results from the spontaneous adsorption. This is the reason why we used a method combining Langmuir trough experiments allowing controlling the surface pressure and an interfacial stress controlled rheometer equipped with a double wall ring (DWR) geometry with openings to ensure homogenous concentrations on both sides of the ring [33,36,37], whose dimensions can be found in [33]. The Teflon homemade Langmuir trough was 780 mm large and 75 mm width. It was equipped with two mobile barriers positioned at 30 mm each from the edge, corresponding to a compressible area of 540 cm². The surface pressure was recorded with a Wilhelmy balance equipped with a paper plate. Knowing the area occupied by the DWR and the mold the effective compressible area was calculated, it was equal to 531.6 cm².

Microgels were spread at the air-water interface as described in [9]. Microgels were first dispersed in a water-isopropanol (5:1) mixture that was then spread at the water surface using a Hamilton syringe and let for one hour.

For each sample, the viscoelastic linear domain (VELD) was determined by varying the oscillating shear strain amplitude from 0.1% to 50% at various surface pressures ranging from 1 to 30 mN/m at a fixed frequency of 0.1 Hz. The evolution of G'^s and G''^s was then recorded, they are defined as:

$$G'^s = \frac{\sigma_0}{\gamma_0}\cos\delta \qquad \text{(Eq. 6a)}$$

$$G''^s = \frac{\sigma_0}{\gamma_0}\sin\delta \qquad \text{(Eq. 6b)}$$

where σ_0 is the 2D stress amplitude, γ_0 the 2D strain amplitude and δ the phase shift. For each rheology experiment, the surface pressure was let to equilibrate for 15 min prior to measurement

and then maintained constant thanks to the Langmuir trough control loop. Once the viscoelastic linear domain determined, frequency sweep experiments were carried out from 0.01 to 1 Hz keeping the strain amplitude in the VELD. Conditions were such that subphase flow corrections do not need to be applied [33].

III) Results and discussion

III.1 Dilational elasticity

Figure 2 reports the apparent dilational elastic and loss moduli deduced from the pendant drop shape analysis at the air-water interface, as a function of pressure for the three cross-linking densities: 1.5, 2.5 and 5 mol%. In all cases, the apparent elastic modulus E'_{app} is much larger than the apparent loss modulus E''_{app}. This elastic dominant behavior is in agreement with results obtained previously for microgel-laden interfaces [12,25,26]. The apparent elastic modulus (as well as the apparent loss modulus in a much lower extent) exhibits a non-monotonous curve going through a maximum noted hereafter $E'_{app\ max}$ for a surface pressure of the order of 14±1 mN/m. The value of $E'_{app\ max}$ strongly increases with the microgels deformability that is to say when the cross-linking density decreases. It is equal to 80, 64 and 50 mN/m for interfaces covered by microgels with 1.5%, 2.5% and 5% of BIS respectively. Note that E''_{app} is almost independent of the cross-linking density. This maximum elasticity occurs in the domain II, corresponding to microgels interacting through their shells.

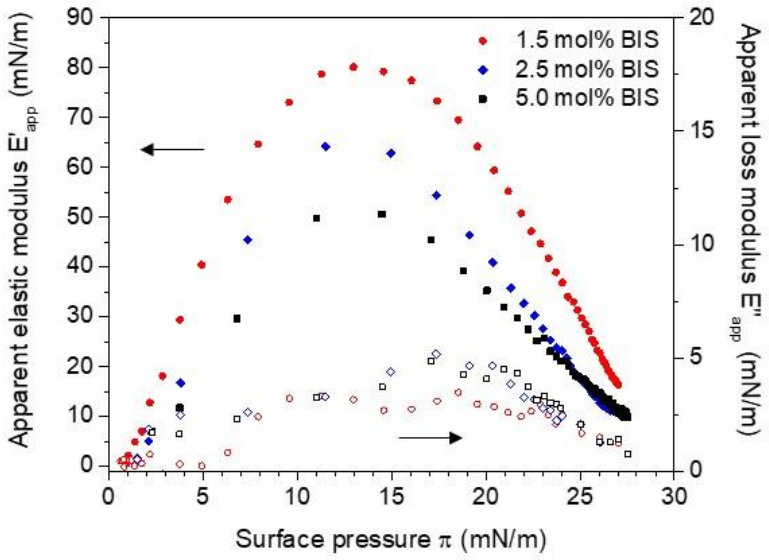

Figure 2**:** Apparent dilational elastic E'$_{app}$ (filled symbols, left axis) and apparent loss E"$_{app}$ (empty symbols, right axis) moduli as a function of the surface pressure measured by the oscillating pendant drop method at the air-water interface for three cross-linking densities (red disks: 1.5 mol%, blue diamonds: 2.5 mol% and black squares: 5 mol%).

Measurements of the apparent elastic modulus (which combines elastic contribution due to microgel compressibility and elastic contribution from interactions between microgels) at oil-water or air-water interfaces with microgels has been shown to be one or two orders of magnitude smaller than the elasticity of interfaces covered by solid undeformable nanoparticles (for which the compressibility contribution is negligible) [25,26,38,39] or the surface plastic stress threshold determined for Pickering emulsions stabilized by silica particles [40]. It is worth noticing that E'$_{app\ max}$ is of the same order as the elastic modulus previously measured by Noskov *et al*. for pNIPAM homopolymer solutions [41].

As discussed previously in the introduction, the shape of the apparent dilational elastic modulus curve as a function of pressure is a consequence of the microgel morphology with a dense and rigid core surrounded by a much softer shell made of dangling chains. Recent studies have focused on local mechanical behavior of individual microgel through dynamic light scattering (DLS), small angle neutron scattering (SANS) and atomic force microscopy (AFM) either

through nano-indentation or peak force nanomechanical mapping (PF-QNM) [42-44]. In particular, Aufderhorst *et al.* have provided evidence of the radial distribution of mechanical properties in the microgel by independently measuring the elasticity of the core and of the shell [43]. The core Young modulus ranged between 17 and 48 kPa, with a higher value as the cross-linking density increased in agreement with a core stiffening with increasing cross-linking. The corona exhibited lower value of the Young modulus, between 3-40 kPa. Notably, for the more densely cross-linked particles, they observed similar moduli because of a significant lower radial heterogeneity, with a much less extended corona. While the elasticity of individual microgels increases with the cross-linking density, Fig. 2 shows the opposite trend for $E'_{app\ max}$ reflecting the importance of the shell rather than the core on the dilation elastic modulus of a microgel assembly. This is also consistent with the fact that this maximum occurs in the domain II where microgels interact through their shells.

III.2 Compression modulus

The Langmuir compression isotherms have been measured for the various cross-linking densities, they are reported in Fig. 3a and transformed into compression elasticity as a function of normalized area A (see Supporting Information SI 3) and as a function of pressure using Eq. 5 (Fig. 3b). The compression rate was fixed at 10 mm/min, the slowest accessible rate. The curves exhibit the classical shape as discussed in the introduction [9,12,45]. One can note the similar general trend as for the dynamic apparent dilational elasticity. The compression modulus E_G exhibits a maximum whose height depends on the amount of cross-linker. The lower the cross-linker amount, the higher the compression modulus. However, the surface pressure corresponding to the maximum elasticity is shifted toward smaller values as it varies from 10±1 to 7±1 mN/m when using microgels with increasing deformability. One can also note that the curves seem less symmetrical with respect to the maximum than the dilational

ones. This could result from a difference of deformation homogeneity in both types of experiments. Indeed the strain in a pendant drop is not purely elongation and shear is present in the neck. Also in the Langmuir through, the type and homogeneity of deformation may depend on the boundary conditions at side walls [46].

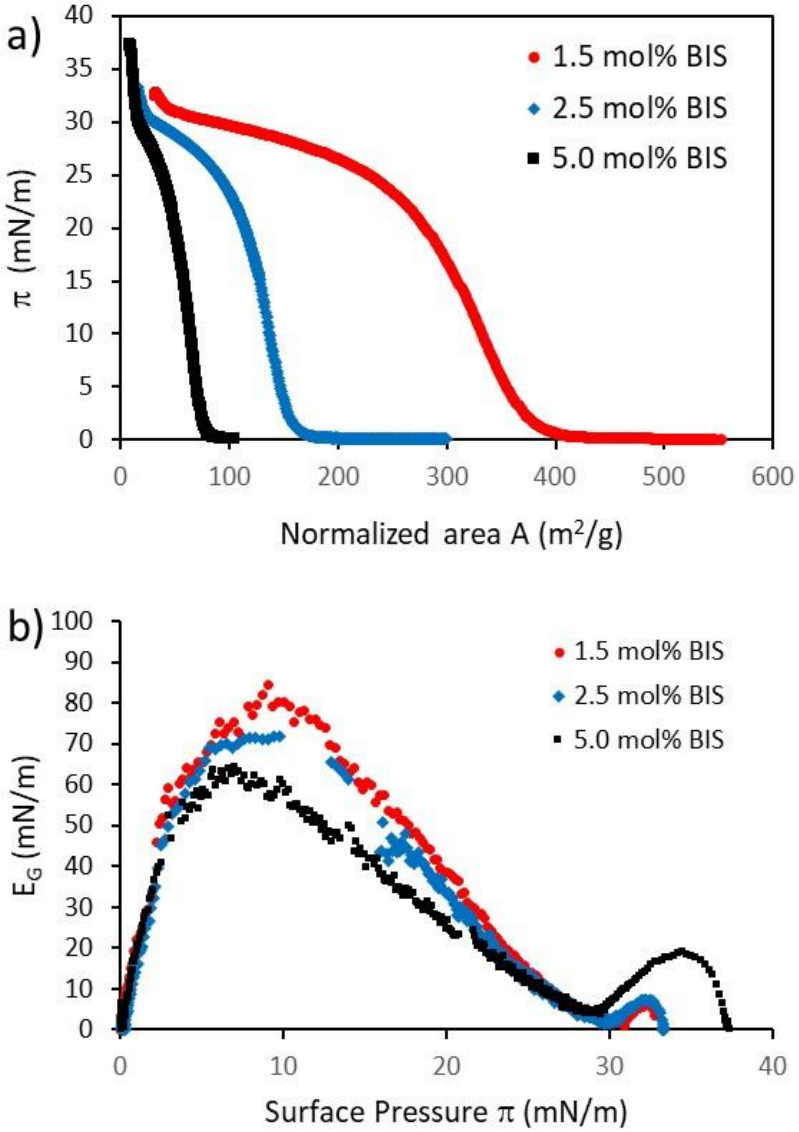

Figure 3: (a) The measured pressure is plotted as a function of normalized area (by the amount of microgels). The experiment is performed at a rate of 10 mm/min. (b) Elastic compression modulus E_G (defined by Eq. 5) as a function of the surface pressure for the three cross-linking densities

At high surface pressures (above 30 mN/m), a second maximum can be observed. It appears in the domain IV where the cores are thought to interact. From Fig. 3b, it can be seen that this

second maximum exhibits an opposite trend. Indeed its amplitude increases as a function of the cross-linking density in agreement with harder cores and occurs at a higher surface pressure for pNIPAM-5. It therefore seems that this secondary maximum originates from the core compressions. The amplitudes of the elastic maxima (compression and dilational ones) are compared in Fig. 4.

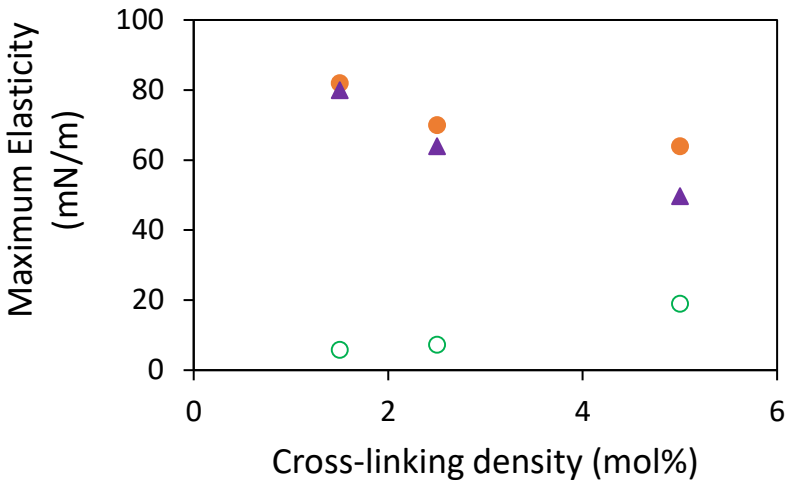

Figure 4: Maximum elastic moduli as a function of the cross-linking density (disks: compression modulus E_G, triangles: dilational apparent elastic modulus E' and empty circles: secondary maximum compression modulus).

III.3 Shear moduli

Despite the fact that the main trends are correctly described, the two previous methods do not allow to fully characterize the mechanical behavior of the interfaces at a controlled pressure in the stationary state. This becomes possible by combining a Langmuir trough and interfacial shear rheology [33,37,47,48]. The experiments have been performed on the pNIPAM-1.5 and pNIPAM-5.

III.3.1 Effect of applied strain at a fixed surface pressure

The VELD was determined by varying the strain amplitude from 0.1% to 20% at a fixed surface pressure from 1 to 28 mN/m (Fig. 5a) at 0.1 Hz. This frequency has been chosen to

cover the same range as the dilation experiments. A larger strain amplitude range has been tested (from 0.01% to 50%). However, at low surface pressure, the experiments were limited by the apparatus detection limit, and at high surface pressure by the monolayer rigidity that led to macroscopically observable inhomogeneous deformation and fracture, consistent with the formation of a predominantly solid interface. This is the reason why in a typical experiment the strain amplitude range was fixed between 0.1 to 20%. In fig. 5b to 5g, G'^{s} and G''^{s} are plotted as a function of the shear strain for the various surface pressures for pNIPAM-1.5 depicted in Fig. 5a.

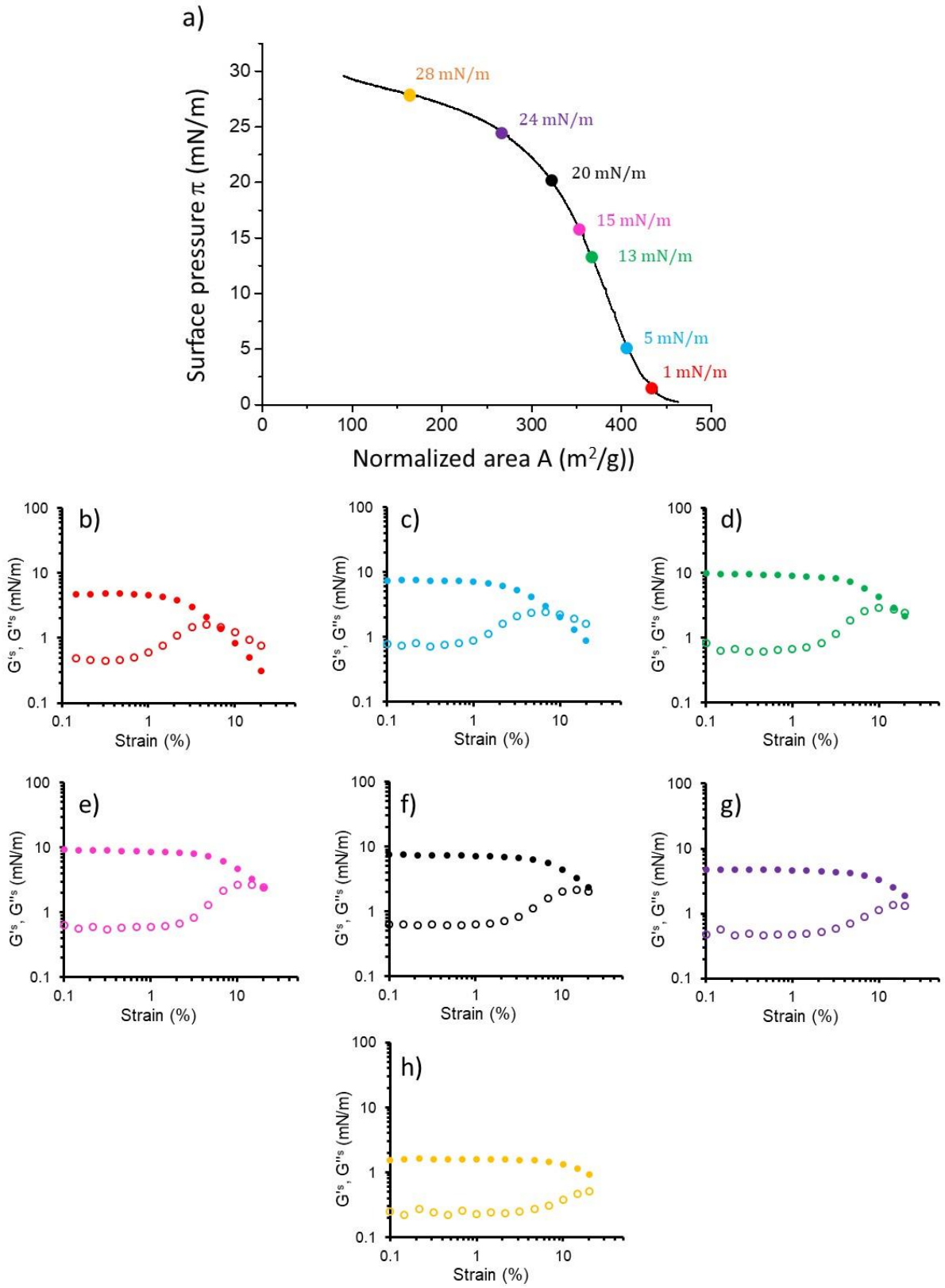

Figure 5: Characterization of the pNIPAM-1.5 laden air-water interface a) Langmuir isotherm, b to h) G'^{s} (full symbols) and G''^{s} (empty symbols) as a function of the strain amplitude at fixed 0.1 Hz frequency for different pressures b) π=1 mN/m, c) π=5 mN/m, d) π=13 mN/m, e) π=15 mN/m, f) π=20 mN/m, g) π=24 mN/m, and h) π=28 mN/m. All the data are superimposed for comparison in see Supporting Information SI 3

Whatever the applied surface pressure, the interface behaves as a viscoelastic solid with G'^{s} larger than G''^{s} by at least one order of magnitude. The evolution of the moduli with the strain amplitude exhibits similar shape for the various pressures. It can be divided into three regions. In the first domain, at low strain (<1%), G'^{s} and G''^{s} are constant (and the stress amplitude varies linearly with the strain amplitude) corresponding to the VELD where G'^{s} and G''^{s} characterize the intrinsic material properties. This linear domain is more extended when the surface pressure increases. In the second domain, G'^{s} begins to decrease while G''^{s} increases until reaching a maximum meaning that the energy dissipation increases. The strain is high enough to induce microgel reorganization: the interface begins to flow. At higher strains, both G'^{s} and G''^{s} decrease, most likely due to sliding between microgels. These shapes are analogous to the ones that are usually observed in bulk rheology for many materials as for example in emulsions [49,50] or colloidal crystals of polystyrene core-PNIPAM shell particles [51]. This confirms the 2D soft glassy material behavior previously proposed from the arrested dynamics [28]. In 3D rheology, this shape, termed "G" overshoot", has been shown to result from the transition from the soli-like to liquid-like behavior in yielding materials [52]. It can therefore be concluded that this is a typical signature of plasticity, also in these 2D microgel layers.

The same experiments have been carried out for the higher cross-linked microgels PNIPAM-5 (see Fig. 6).

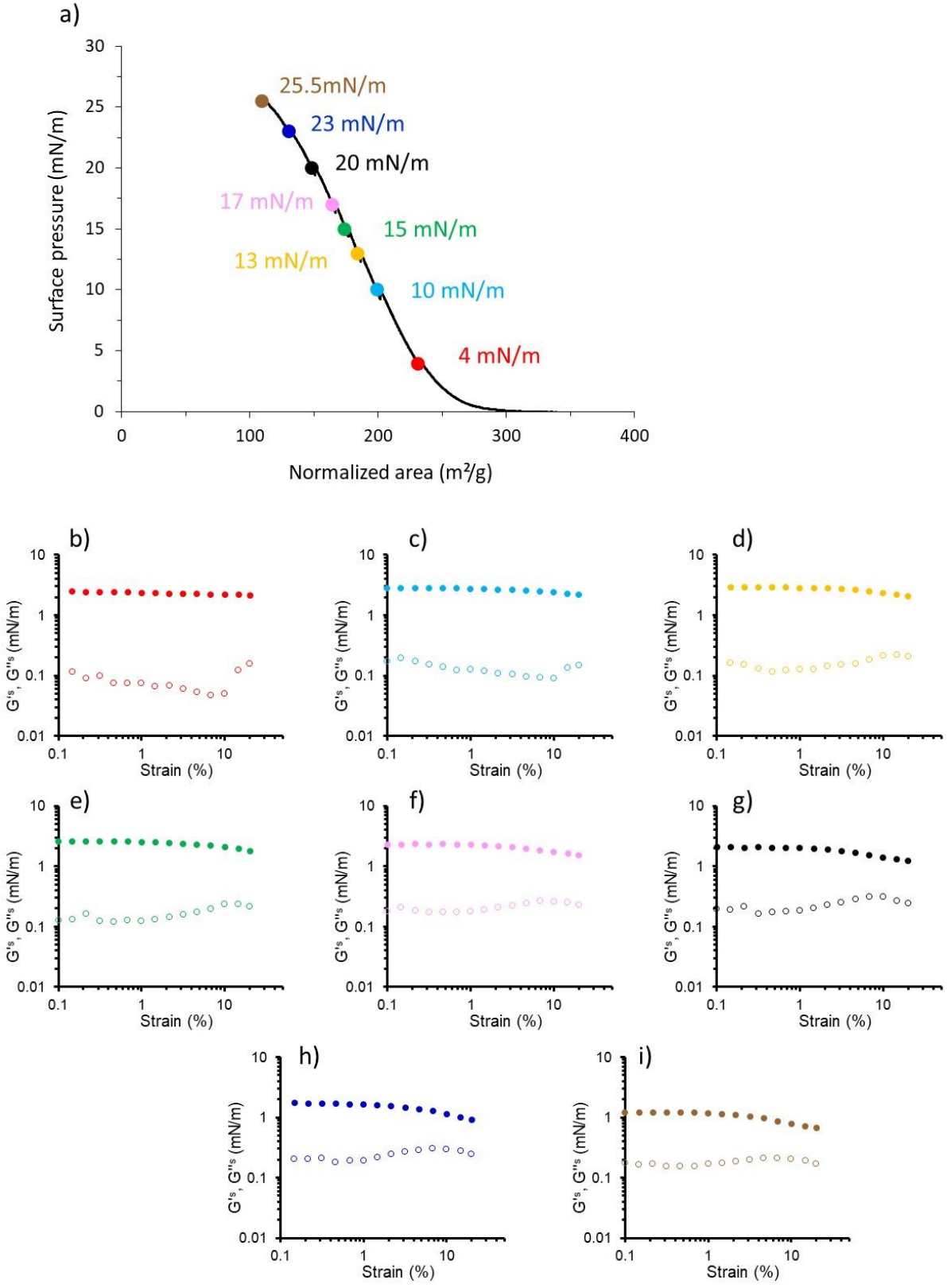

Figure 6: Characterization of the PNIPAM-5 laden air-water interface a) Langmuir isotherm, b to i) G'^{s} (full symbols) and G''^{s} (empty symbols) as a function of the strain amplitude at fixed 0.1 Hz frequency for different pressures b) π=4 mN/m, c) π=10 mN/m, d) π=13 mN/m, e) π=15 mN/m, f) π=17 mN/m, g) π=20 mN/m, h) π=23 mN/m and i) π=25.5 mN/m. All the date are superimposed in see Supporting Information SI 4.

As for the less cross-linked microgels, the pNIPAM-5 laden interface exhibits a solid-dominant behavior as G'^{s} is much larger than G''^{s} in the whole explored pressure range. However, the values of both elastic and loss moduli are weaker than for the more deformable microgels ($G'^{s} \approx 10$ mN/m for pNIPAM-1.5 at maximum and $G'^{s} \approx 3$ mN/m for pNIPAM-5 at maximum). It can also be noticed that no crossover between G'^{s} and G''^{s} can be seen and that the linear domain is even less extended that the surface pressure increases. The overshoot of G''^{s} is also less noticeable suggesting that the flow setting corresponds to less energy dissipation.

III.3.2 Effect of frequency

At a fixed strain belonging to the linear domain in all cases (0.5%), a frequency sweep (from 0.01 to 1 Hz) was performed for various surface pressures. The results are reported in Fig. 7 a and b for pNIPAM-1.5 and pNIPAM-5. They are also plotted on a single graph in Supporting Information SI 4 and SI 5 for pNIPAM-1.5 and pNIPAM-5 respectively.

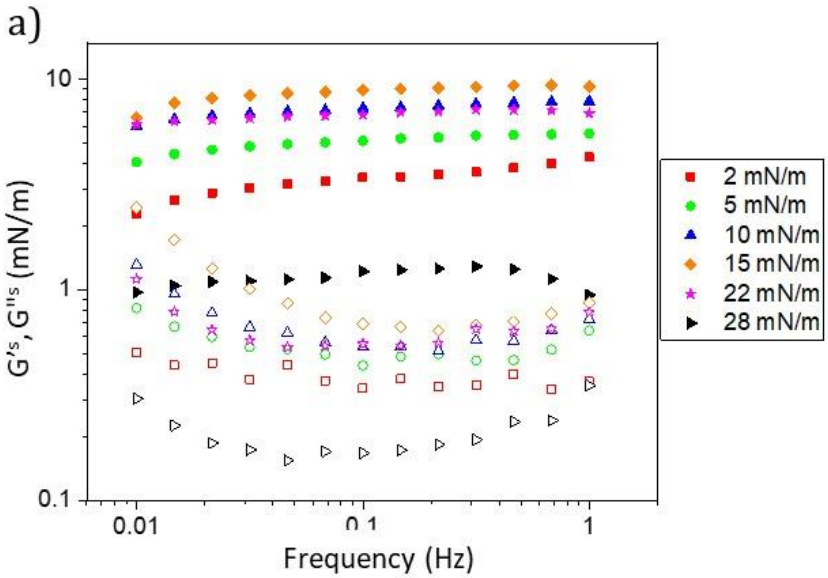

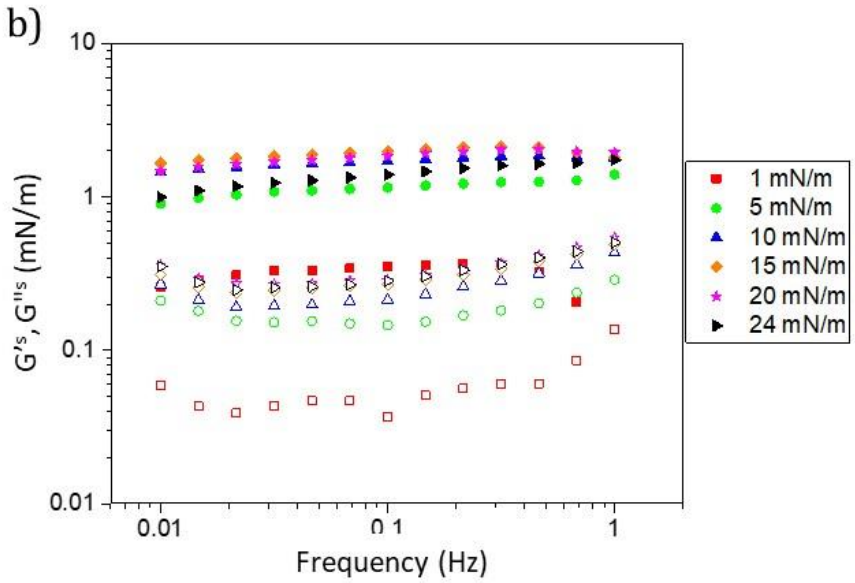

Figure 7: Surface elastic modulus G's (full symbols) and surface loss modulus G"s (empty symbols) as a function of the frequency. The applied strain is equal to 0.5%. a) pNIPAM-1.5 and b) pNIPAM-5.

In all cases, for both cross-linking densities and for all surface pressures, G'^{s} is independent of the applied frequency and remains much larger than G''^{s} showing the main solid behavior in the whole frequency range. The loss modulus exhibits a minimum and increases at higher frequency. For pNIPAM-5, this minimum seems to be shallower.

The same frequency behavior has been observed by Petekidis *et al.* [51] in pNIPAM hydrogels films. It has been identified as a solid behavior of hard spheres. In 3D rheology, such frequency dependence is common, for example in concentrated colloidal suspensions or emulsions. In these systems, each particle or drop is seen as trapped in a cage formed by its neighbors. Mason and Weitz have shown that this minimum in G", in 3D, originates from the existence of two distinct characteristic times: the shortest time characterizes the particle motion dynamics inside the cage while the longer time corresponds to the cage relaxation [53].

The previous results can also be presented as a function of the surface pressure.

III.3.3 Effect of the surface pressure

From the shear measurements, we can extract the characteristic parameters G'^s, G''^s, γ_c^s and σ_c^s. We define the critical strain γ_c^s and σ_c^s as the limit of the VELD. For that, we plotted the oscillating stress amplitude as a function of the oscillating strain amplitude, the critical values γ_c^s and σ_c^s are taken as the last point before deviation for the linear relation between both amplitudes (an example is given in supporting information SI 6). After this limit, a deviation with respect to linearity is observed.

Fig. 8 reports G'^s and G''^s as a function of the surface pressure for the two cross-linking densities.

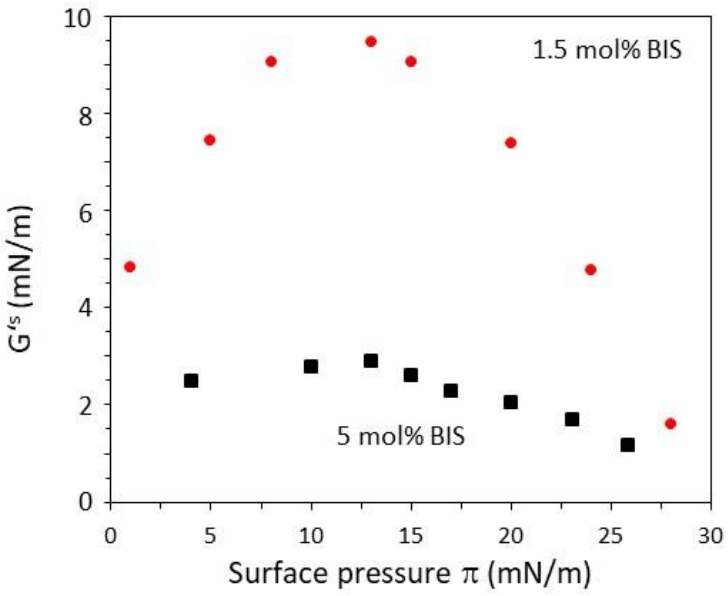

Figure 8: Magnitude of the elastic shear plateau surface modulus G'^s as a function of surface pressure for microgels with two different cross-linking densities 1.5 (red disks) and 5 mol% (black squares) of BIS.

The same shape can be observed for G'^s as for apparent E'_{app} and E_G. The magnitude of the surface shear modulus goes through a maximum as a function of the surface pressure. To allow

better comparison, Table 2 lists the maximum elasticity values of G'^{s}_{max}, $E_{G_{max}}$ and $E'_{app\ max}$ of G'^{s}, E_G and E'_{app} respectively as well as the corresponding surface pressure π_{max}.

Table 2: Summary of the maximal values of elasticity obtained with the three methods. All the moduli and pressures are expressed in mN/m.

	Apparent dilational elasticity		Interfacial shear rheology		Compression using a Langmuir trough		Ratio $E'_{app\ max}/G'^{s}_{max}$	Ratio $E_{G\ max}/G'^{s}_{max}$
	$E'_{app\ max}$	π_{max}	G'^{s}_{max}	π_{max}	$E_{G_{max}}$	π_{max}		
PNIPAM-1.5	80	13	9.5	13	82	9	8.5	8.6
PNIPAM-5	50	13	3	13	64	9	16.7	21

Whatever the method, the magnitudes of the maxima in the elastic moduli G'^{s}_{max} and $E'_{app\ max}$ are larger for the interfaces created with the more deformable microgels than for the more rigid ones. Moreover, the maximum arises for the same surface pressure indicating that the interface has a similar response independently of the way it is solicited (dilatation or shear or even complex combinations of both since for the pendant drop and Langmuir trough the deformations are not pure). One can also notice that dilational and shear moduli take different values with E'_{app} larger than G'^{s} by almost an order of magnitude. However, as demonstrated by Brugger *et al*. on pNIPAM-co-AA [25], differences may exist between results obtained by dilational and shear rheology. The authors justified this observation by the fact that the interactions that are measured by the two methods are not necessarily the same: shear rheology measures the response to (translation) rotation and elongation of the interface while dilational rheology is sensitive to the ability of the layer to adapt its lattice parameter (distance between microgels) under the effect of expansion-compression. Consequently, one can imagine that in our case, the elastic interface response to a shear or a dilatation is not the same. Then shear and dilational rheology allows mechanically stressing the microgel-laden interface with two stimuli:

(com)pression or shear strain. Making an analogy with three-dimensional mechanics and the Poisson coefficient, as the ratios $E'_{app\ max}/G'^{s}_{max}$ as well as $E_{G\ max}/G'^{s}_{max}$ differ for both types of microgels (Table 2), this could indicate intrinsic differences of the two materials.

The values of γ_c^s and σ_c^s are plotted as a function of the surface pressure in Fig. 9 and in Supporting Information SI7.

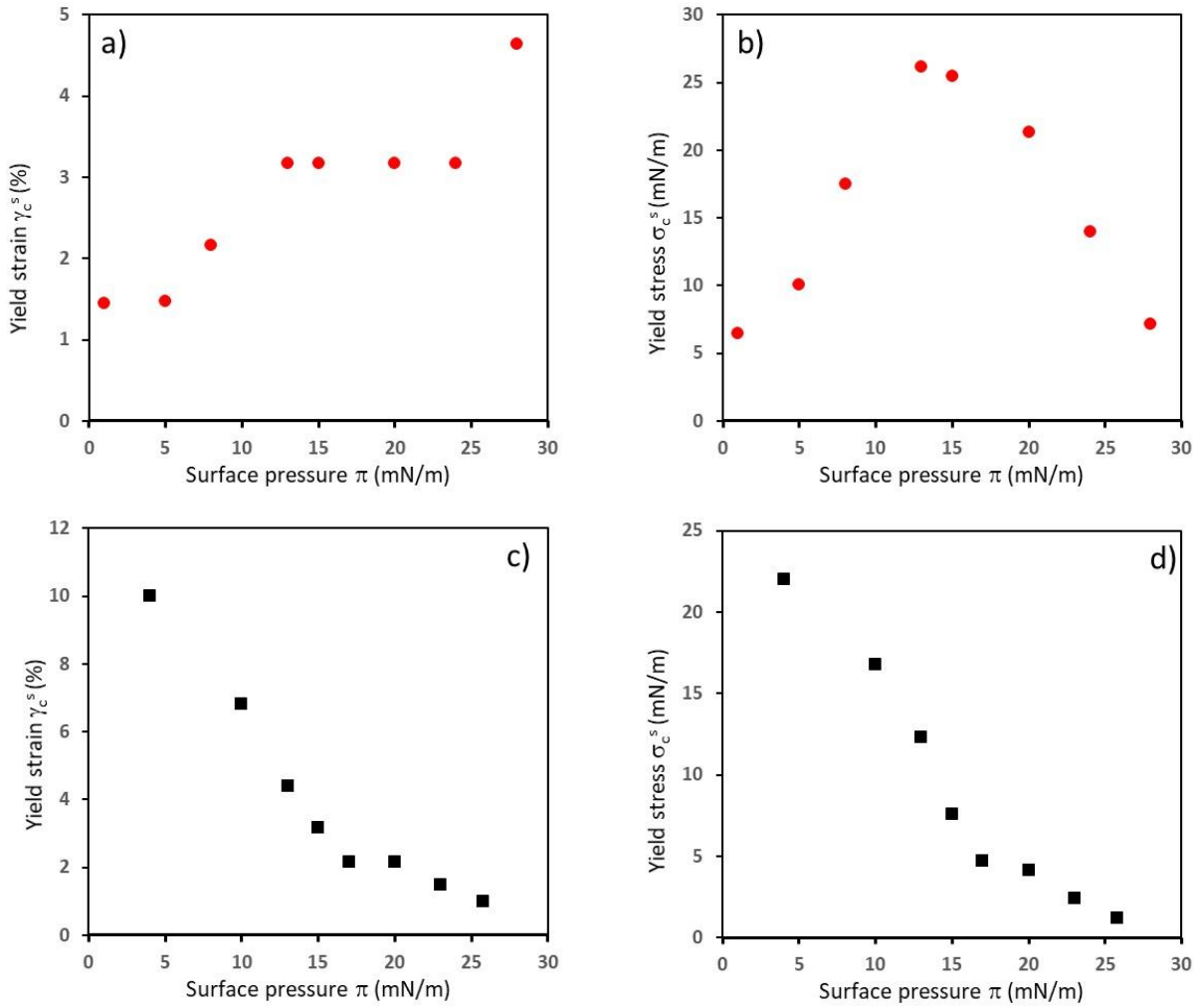

Figure 9: Variation of a, c) the critical strain γ_c^s and b, d) corresponding stress σ_c^s as a function of the surface pressure imposed in the Langmuir trough for a, b) pNIPAM-1.5 and c, d) pNIPAM-5. The data are superimposed for comparison in see Supporting Information SI 7.

Fig. 9a highlights the fact that for pNIPAM-1.5 the critical strain increases with the surface pressure in a quite narrow range, from about 1.5% at π=1 mN/m where microgels are packed

in a hexagonal array with peripheral chains that begin to interact, up to about 5% when the pressure is close to 30 mN/m. It therefore seems that it is easier to "break" the hexagonal lattice and to make it flow at low pressures. The corresponding stress increases progressively and reaches a maximum value at about 25 mN/m before decreasing at higher surface pressures.
From fig. 9c, a major difference can be observed for the higher cross-linked microgels: in opposition to pNIPAM-1.5, the VELD for pNIPAM-5 is all the narrower that the surface pressure increases, indeed γ_c decreases when surface pressure increases.

As the surface elastic modulus G'^s is always larger than the loss modulus by more than a decade, the contribution of the loss modulus to the total viscoelastic modulus can be neglected. Then, the stress maximum, during stationary oscillatory deformations, is approximately given by the elastic modulus times the strain amplitude $\sigma^s = \gamma^s \times G'^s$. For pNIPAM-1.5, the critical stress for such oscillatory deformations is the product of the critical strain amplitude, which is an increasing function of the surface pressure, times the elastic modulus that exhibits a maximum. Therefore, the critical stress exhibits the same shape as the elastic modulus, an increase until a maximum and then a decrease. In contrast for the higher cross-linked pNIPAM-5 microgels, the elastic modulus varies much less, so that the critical stress exhibits a similar shape than the critical strain that is to say a decrease when the surface pressure increases. This seems indicating that below the maximum pressure, the shear-induced transition from solid-like to liquid-like behavior is dominated by the elasticity originating from interpenetrating microgels through their shells for the more deformable microgels. In the case of more cross-linked microgels, as the yield stress is larger for low surface pressure, rearrangement and sliding phenomena, induced by large deformation prevail, and are likely responsible for the irreversible plastic deformation.

IV. Conclusion

Microgels have been shown to strongly adsorb at liquid interfaces by flattening [5-10] with a main protrusion towards water [5]. As a consequence of their core-shell structure [11], they are able to densely cover the drop surface by adopting a fried-egg like morphology, thereby stabilizing emulsions [6]. It is known that the emulsions are all the more mechanically resistant as the microgel deformability increases [6]. This has been connected to the interfacial properties of the microgels. Langmuir compression experiments combined with AFM observations showed a complex microstructural evolution, with the existence of five domains when increasing the surface coverage going from a dilute 2D gas of microgel particles (domain I) all the way to the interface buckling (domain V). However, only few experiments were previously performed to assess the mechanical behavior of microgel-laden interfaces [8,12,25-28], and an integral view is missing. So far, the surface elastic modulus was derived from oscillation of a pendant drop [12,25,27] or from micro-rheology [8,25,26,28]. In such experiments, applied deformations however constitute complex and mixed deformation fields, with the amount of shear and dilation depending on the very properties one tries to measure. In the present work, the mechanical properties of model interfaces covered by microgel particles have been studied by an array of techniques, to elucidate the full rheological response of the interface. The experiments included pendant drop oscillation and Langmuir compression and a complete shear rheology study was performed using a double wall ring cell mounted onto a Langmuir through. The latter enables one to measure the response to controlled simple shear deformations at controlled pressure/surface coverage in static conditions. This is the first time such an integral view on the rheology of microgel interfaces is reported. Moreover the effect of the microgel deformability, meaning the impact of the cross-linker concentration during synthesis, on the shear rheology has been examined.

The elastic response of adsorbed microgels at the air/water interface was established as a function of surface pressure. Whatever the method used, the magnitude of the different elastic moduli goes through a maximum of elasticity for pressure values of about 10-15 mN/m confirming previously reported trends [8,9,12]. This behavior is a direct consequence of the particular structure of microgels, *i.e.* a dense and rigid core surrounded by a deformable shell made of dangling chains. The presence of an elastic maximum can be rationalized by a conformational change of the hydrophobic segments of pNIPAM microgels constituting the shell from a proximal region (polymer layer) to a so-called distal region. At the beginning of the adsorption process, the dangling chains are likely organized parallel to the surface. An increase in particle concentration or equivalently in surface pressure causes the chains to fold in the distal region of the polymer layer. A stress relaxation can then occur due to a conformational exchange of the polymer segments, which can desorb from the surface (proximal region) to form loops in the distal region. The elastic contribution of the loops being less important than that of the segments adsorbed on the surface, it results in a decrease of the elastic modulus when the interface is further compressed. The elastic modulus is lower for higher cross-linking density, likely resulting from the fact that the less the microgels are cross-linked, the higher the contribution of the chains constituting the shell. An additional study would be required to identify the role of local entanglements (chains constituting the shell and having a free end able to interact with the chains of the neighboring microgels) on the mechanical properties of dispersion of microgels at different cross-linking rates.

A secondary elastic maximum is observed at high surface pressures (above 30 mN/m) as already seen in [27,28]. We herein showed that its amplitude increases when the cross-linking density increases, corresponding to an opposite trend compared to the first maximum but in agreement with individual microgel rigidity [43]. Since, at such high surface pressures, microgels interact

through core-core interaction, this secondary maximum is likely originating from the core-core Hertzian interactions, as hypothesized in [13] and referred in [28].

One has also to be aware of some fundamental differences when comparing liquid interfaces properties. In the case of spontaneous adsorption, microgels spontaneously adsorb at high surface pressures (close to 30 mN/m) corresponding to the end of domain III [12,14], above the first elastic maximum and below the secondary elastic maximum. In the case of forced compression, the whole surface coverage or equivalently the whole microgel conformation range is accessible. In the case of emulsion drops, when emulsification is performed in the particle-poor domain, it has been shown that microgels are flattened, their shells are interpenetrated while their cores are not in contact [6] which corresponds to the domain II defined for the model interfaces. This domain, characterized by interacting shells, is very extended in surface pressure and the elasticity goes through a maximum. It should be noted that this maximum of elasticity occurs for a given pressure whatever the microgels cross-linking density and for various surface coverage corresponding to various center-to-center distance between microgels. In the emulsions, it has been shown that, due to higher microgel deformability, the microgels flattening increases when the cross-linking density decreases, keeping a constant center-to-center distance between microgels [6]. To allow a complete conclusion it should be necessary to assess the surface pressure of the drop composing the emulsions.

The present reported shear study on model interfaces brings clarity on the dominant solid behavior with G'^{s} larger than G''^{s} , in the viscoelastic linear domain, whatever the applied pressure and whatever the frequency in the explored range. G'^{s} is independent of the frequency while G''^{s} goes trough a minimum. By analogy with 3D rheology [53], we suggest that this minimum originates from the existence of two characteristic times, the shortest one corresponding to the microgel dynamics in its cage formed by neighboring microgels while the

longest time represents the cage relaxation. For increasing shear strains, exiting the viscoelastic linear domain, we also showed the influence of the microgel deformability. Indeed, the viscoelastic linear domain extended for increasing surface pressures for interfaces covered by the more deformable microgels while it reduced for interfaces covered by the more rigid ones. In all cases, the interfaces exhibit a elasto-plastic behavior whose yield stress seems to be dominated by the elasticity going through a maximum as a function of surface pressure for the more deformable microgels while the yield stress seems to be dominated by shear-induced rearrangements that become easier as the surface pressure increases in the case of more rigid microgels. In our opinion, the most challenging question that now arises is the transposition of these model interface rheological characterization to interfaces present in emulsion systems and to the macroscopic properties of emulsions.

ACKNOWLEDGMENTS

This work was supported by the CNRS, the University of Bordeaux and Bordeaux INP. The authors would like to thanks the European Soft Matter Infrastructure (EUSMI) network for funding MCT's stay at ETH Zürich.

REFERENCES

1. Pelton, R., *Temperature-Sensitive Aqueous Microgels.* Advances in Colloid and Interface Science, 2000. **85**(1): p. 1-33 DOI: https://doi.org/10.1016/S0001-8686(99)00023-8.
2. Zhang, J. and Pelton, R., *The Dynamic Behavior of Poly(N-Isopropylacrylamide) at the Air/Water Interface.* Colloids and Surfaces A: Physicochemical and Engineering Aspects, 1999. **156**(1): p. 111-122 DOI: https://doi.org/10.1016/S0927-7757(99)00063-1.
3. Serpe, M.J., Kim, J. and Lyon, L.A., *Colloidal Hydrogel Microlenses.* Advanced Materials, 2004. **16**(2): p. 184-187 DOI: https://doi.org/10.1002/adma.200305675.
4. Rey, M., Fernandez-Rodriguez, M.A., Karg, M., Isa, L. and Vogel, N., *Poly- N-Isopropylacrylamide Nanogels and Microgels at Fluid Interfaces.* Accounts of Chemical Research, 2020 53 (2): p414-424 DOI: https://doi.org/10.1021/acs.accounts.9b00528.
5. Richtering, W., *Responsive Emulsions Stabilized by Stimuli-Sensitive Microgels: Emulsions with Special Non-Pickering Properties.* Langmuir, 2012. **28**(50): p. 17218-17229 DOI: https://doi.org/10.1021/la302331s.
6. Destribats, M., Lapeyre, V., Wolfs, M., Sellier, E., Leal-Calderon, F., Ravaine, V. and Schmitt, V., *Soft Microgels as Pickering Emulsion Stabilisers: Role of Particle Deformability.* Soft Matter, 2011. **7**(17): p. 7689-7698 DOI: https://doi.org/10.1039/C1SM05240C.
7. Style, R.W., Isa, L. and Dufresne, E.R., *Adsorption of Soft Particles at Fluid Interfaces.* Soft Matter, 2015. **11**(37): p. 7412-7419 DOI: https://doi.org/10.1039/C5SM01743B.
8. Rey, M., Fernández-Rodríguez, M.Á., Steinacher, M., Scheidegger, L., Geisel, K., Richtering, W., Squires, T.M. and Isa, L., *Isostructural Solid–Solid Phase Transition in Monolayers of Soft Core–Shell Particles at Fluid Interfaces: Structure and Mechanics.* Soft Matter, 2016. **12**(15): p. 3545-3557 DOI: https://doi.org/10.1039/C5SM03062E.
9. Picard, C., Garrigue, P., Tatry, M.-C., Lapeyre, V., Ravaine, S., Schmitt, V. and Ravaine, V., *Organization of Microgels at the Air–Water Interface under Compression: Role of Electrostatics and Cross-Linking Density.* Langmuir, 2017. **33**(32): p. 7968-7981 DOI: https://doi.org/10.1021/acs.langmuir.7b01538.
10. Camerin, F., Fernández-Rodríguez, M.Á., Rovigatti, L., Antonopoulou, M.-N., Gnan, N., Ninarello, A., Isa, L. and Zaccarelli, E., *Microgels Adsorbed at Liquid–Liquid*

Interfaces: A Joint Numerical and Experimental Study. ACS Nano, 2019. **13**(4): p. 4548-4559 DOI: https://doi.org/10.1021/acsnano.9b00390.
11. Wu, X., Pelton, R.H., Hamielec, A.E., Woods, D.R. and McPhee, W., *The Kinetics of Poly(N-Isopropylacrylamide) Microgel Latex Formation.* Colloid and Polymer Science, 1994. **272**(4): p. 467-477 DOI: https://doi.org/10.1007/BF00659460.
12. Pinaud, F., Geisel, K., Massé, P., Catargi, B., Isa, L., Richtering, W., Ravaine, V. and Schmitt, V., *Adsorption of Microgels at an Oil-Water Interface: Correlation between Packing and 2d Elasticity.* Soft Matter, 2014. **10**(36): p. 6963-6974 DOI: https://doi.org/10.1039/c4sm00562g.
13. Maldonado-Valderrama, J., del Castillo-Santaella, T., Adroher-Benítez, I., Moncho-Jordá, A. and Martín-Molina, A., *Thermoresponsive Microgels at the Air–Water Interface: The Impact of the Swelling State on Interfacial Conformation.* Soft Matter, 2017. **13**(1): p. 230-238 DOI: https://doi.org/10.1039/C6SM01375A.
14. Tatry, M.C., Laurichesse, E., Perro, A., Ravaine, V. and Schmitt, V., *Kinetics of Spontaneous Microgels Adsorption and Stabilization of Emulsions Produced Using Microfluidics.* Journal of Colloid and Interface Science, 2019. **548**: p. 1-11 DOI: https://doi.org/10.1016/j.jcis.2019.04.020.
15. Fujii, S., Read, E.S., Binks, B.P. and Armes, S.P., *Stimulus-Responsive Emulsifiers Based on Nanocomposite Microgel Particles.* Advanced Materials, 2005. **17**(8): p. 1014-1018 DOI: https://doi.org/10.1002/adma.200401641.
16. Ngai, T., Behrens, S.H. and Auweter, H., *Novel Emulsions Stabilized by Ph and Temperature Sensitive Microgels.* Chemical Communications, 2005. **3**: p. 331-333 DOI: https://doi.org/10.1039/B412330A.
17. Fujii, S., Armes, S.P., Binks, B.P. and Murakami, R., *Stimulus-Responsive Particulate Emulsifiers Based on Lightly Cross-Linked Poly(4-Vinylpyridine)−Silica Nanocomposite Microgels.* Langmuir, 2006. **22**(16): p. 6818-6825 DOI: https://doi.org/10.1021/la060349l.
18. Ngai, T., Auweter, H. and Behrens, S.H., *Environmental Responsiveness of Microgel Particles and Particle-Stabilized Emulsions.* Macromolecules, 2006. **39**(23): p. 8171-8177 DOI: https://doi.org/10.1021/ma061366k.
19. Brugger, B., Rosen, B.A. and Richtering, W., *Microgels as Stimuli-Responsive Stabilizers for Emulsions.* Langmuir, 2008. **24**(21): p. 12202-12208 DOI: https://doi.org/10.1021/la8015854.
20. Brugger, B. and Richtering, W., *Emulsions Stabilized by Stimuli-Sensitive Poly(N-Isopropylacrylamide)-Co-Methacrylic Acid Polymers: Microgels Versus Low Molecular Weight Polymers.* Langmuir, 2008. **24**(15): p. 7769-7777 DOI: https://doi.org/10.1021/la800522h.
21. Schmitt, V. and Ravaine, V., *Surface Compaction Versus Stretching in Pickering Emulsions Stabilised by Microgels.* Current Opinion in Colloid and Interface Science, 2013. **18**(6): p. 532-541 DOI: https://doi.org/10.1016/j.cocis.2013.11.004.
22. Tatry, M.-C., Qiu, Y., Lapeyre, V., Garrigue, P., Schmitt, V. and Ravaine, V., *Sugar-Responsive Pickering Emulsions Mediated by Switching Hydrophobicity in Microgels.* Journal of Colloid and Interface Science, 2020. **561**: p. 481-493 DOI: https://doi.org/10.1016/j.jcis.2019.11.023.
23. Tatry, M.-C., Galanopoulo, P., Waldmann, L., Lapeyre, V., Garrigue, P., Schmitt, V. and Ravaine, V., *Pickering Emulsions Stabilized by Thermoresponsive Oligo(Ethylene Glycol)-Based Microgels: Effect of Temperature-Sensitivity on Emulsion Stability.* Journal of Colloid and Interface Science, 2021. **589**: p. 96-109 DOI: https://doi.org/10.1016/j.jcis.2020.12.082.

24. Ata, S., Davis, E.S., Dupin, D., Armes, S.P. and Wanless, E.J., *Direct Observation of Ph-Induced Coalescence of Latex-Stabilized Bubbles Using High-Speed Video Imaging.* Langmuir, 2010. **26**(11): p. 7865-7874 DOI: https://doi.org/10.1021/la904708x.
25. Brugger, B., Vermant, J. and Richtering, W., *Interfacial Layers of Stimuli-Responsive Poly-(N-Isopropylacrylamide-Co-Methacrylicacid) (Pnipam-Co-Maa) Microgels Characterized by Interfacial Rheology and Compression Isotherms.* Physical Chemistry Chemical Physics, 2010. **12**(43): p. 14573-14578 DOI: https://doi.org/10.1039/C0CP01022G.
26. Cohin, Y., Fisson, M., Jourde, K., Fuller, G.G., Sanson, N., Talini, L. and Monteux, C., *Tracking the Interfacial Dynamics of Pnipam Soft Microgels Particles Adsorbed at the Air–Water Interface and in Thin Liquid Films.* Rheologica Acta, 2013. **52**(5): p. 445-454 DOI: https://doi.org/10.1007/s00397-013-0697-3.
27. Akentiev, A.V., Rybnikova, G.S., Novikova, A.A., Timoshen, K.A., Zorin, I.M. and Noskov, B.A., *Dynamic Elasticity of Films Formed by Poly(N-Isopropylacrylamide) Microparticles on a Water Surface.* Colloid Journal, 2017. **79**(5): p. 571-576 DOI: https://doi.org/10.1134/S1061933X17050027.
28. Huang, S., Gawlitza, K., von Klitzing, R., Steffen, W. and Auernhammer, G.K., *Structure and Rheology of Microgel Monolayers at the Water/Oil Interface.* Macromolecules, 2017. **50**(9): p. 3680-3689 DOI: https://doi.org/10.1021/acs.macromol.6b02779.
29. Guillermic, R.-M. and Saint-Jalmes, A., *Dynamics of Poly-Nipam Chains in Competition with Surfactants at Liquid Interfaces: From Thermoresponsive Interfacial Rheology to Foams.* Soft Matter, 2013. **9**(4): p. 1344-1353 DOI: https://doi.org/10.1039/C2SM26666K.
30. Yang, Y., Maldonado-Valderrama, J. and Martín-Molina, A., *Temperature and Electrostatics Effects on Charged Poly(N-Isopropylacrylamide) Microgels at the Interface.* Journal of Molecular Liquids, 2020. **303**: p. 112678 DOI: https://doi.org/10.1016/j.molliq.2020.112678.
31. Destribats, M. *Emulsions Stabilized by Stimuli-Responsive Colloidal Particles: Fundamental Properties and Materials*. 2010, Univeristy of Bordeaux, Number: 4151.
32. Lele, A.K., Hirve, M.M., Badiger, M.V. and Mashelkar, R.A., *Predictions of Bound Water Content in Poly(N-Isopropylacrylamide) Gel.* Macromolecules, 1997. **30**(1): p. 157 DOI: https://doi.org/10.1021/ma950894l.
33. Jaensson, N. and Vermant, J., *Tensiometry and Rheology of Complex Interfaces.* Current Opinion in Colloid & Interface Science, 2018. **37**: p. 136-150 DOI: https://doi.org/10.1016/j.cocis.2018.09.005.
34. Nagel, M., Tervoort, T.A. and Vermant, J., *From Drop-Shape Analysis to Stress-Fitting Elastometry.* Advances in Colloid and Interface Science, 2017. **247**: p. 33-51 DOI: https://doi.org/10.1016/j.cis.2017.07.008.
35. Bischofberger, I., Calzolari, D.C.E., De Los Rios, P., Jelezarov, I. and Trappe, V., *Hydrophobic Hydration of Poly-N-Isopropyl Acrylamide: A Matter of the Mean Energetic State of Water.* Scientific Reports, 2014. **4**(1): p. 4377 1-6 DOI: https://doi.org/10.1038/srep04377.
36. Vandebril, S., Franck, A., Fuller, G.G., Moldenaers, P. and Vermant, J., *A Double Wall-Ring Geometry for Interfacial Shear Rheometry.* Rheologica Acta, 2010. **49**(2): p. 131-144 DOI: https://doi.org/10.1007/s00397-009-0407-3.

37. Pepicelli, M., Verwijlen, T., Tervoort, T.A. and Vermant, J., *Characterization and Modelling of Langmuir Interfaces with Finite Elasticity.* Soft Matter, 2017. **13**(35): p. 5977-5990 DOI: https://doi.org/10.1039/C7SM01100H.
38. Li, Z., Richtering, W. and Ngai, T., *Poly(N-Isopropylacrylamide) Microgels at the Oil–Water Interface: Temperature Effect.* Soft Matter, 2014. **10**(33): p. 6182-6191 DOI: https://doi.org/10.1039/C4SM00888J.
39. Noskov, B.A., Noskov, B.A. and Bykov, A.G., *Dilational Rheology of Monolayers of Nano- and Micropaticles at the Liquid-Fluid Interfaces.* Current Opinion in Colloid & Interface Science, 2018. **37**: p. 1-12 DOI: https://doi.org/10.1016/j.cocis.2018.05.001.
40. Arditty, S., Schmitt, V., Lequeux, F. and Leal-Calderon, F., *Interfacial Properties in Solid-Stabilized Emulsions.* European Physical Journal B, 2005. **44**(3): p. 381-393 DOI: https://doi.org/10.1140/epjb/e2005-00137-0.
41. Noskov, B.A., Akentiev, A.V., Bilibin, A.Y., Grigoriev, D.O., Loglio, G., Zorin, I.M. and Miller, R., *Dynamic Surface Properties of Poly(N-Isopropylacrylamide) Solutions.* Langmuir, 2004. **20**(22): p. 9669-9676 DOI: https://doi.org/10.1140/10.1021/la048836t.
42. Backes, S. and von Klitzing, R., *Nanomechanics and Nanorheology of Microgels at Interfaces.* Polymers, 2018. **10**(9) 1-23 DOI: https://doi.org/10.3390/polym10090978.
43. Aufderhorst-Roberts, A., Baker, D., Foster, R.J., Cayre, O., Mattsson, J. and Connell, S.D., *Nanoscale Mechanics of Microgel Particles.* Nanoscale, 2018. **10**(34): p. 16050-16061 DOI: https://doi.org/10.1039/C8NR02911C.
44. Witte, J., Kyrey, T., Lutzki, J., Dahl, A.M., Houston, J., Radulescu, A., Pipich, V., Stingaciu, L., Kühnhammer, M., Witt, M.U., Von Klitzing, R., Holderer, O. and Wellert, S., *A Comparison of the Network Structure and Inner Dynamics of Homogeneously and Heterogeneously Crosslinked Pnipam Microgels with High Crosslinker Content.* Soft Matter, 2019. **15**(5): p. 1053-1064 DOI: https://doi.org/10.1039/c8sm02141d.
45. Mendoza, A.J., Guzmán, E., Martínez-Pedrero, F., Ritacco, H., Rubio, R.G., Ortega, F., Starov, V.M. and Miller, R., *Particle Laden Fluid Interfaces: Dynamics and Interfacial Rheology.* Advances in Colloid and Interface Science, 2014. **206**: p. 303-319 DOI: https://doi.org/10.1016/j.cis.2013.10.010.
46. Vora, S.R., Bognet, B., Patanwala, H.S., Young, C.D., Chang, S.Y., Daux, V. and Ma, A.W.K., *Global Strain Field Mapping of a Particle-Laden Interface Using Digital Image Correlation.* Journal of Colloid and Interface Science, 2018. **509**: p. 94-101 DOI: https://doi.org/10.1016/j.jcis.2017.08.082.
47. Van Hooghten, R., Blair, V.E., Vananroye, A., Schofield, A.B., Vermant, J. and Thijssen, J.H.J., *Interfacial Rheology of Sterically Stabilized Colloids at Liquid Interfaces and Its Effect on the Stability of Pickering Emulsions.* Langmuir, 2017. **33**(17): p. 4107-4118 DOI: https://doi.org/10.1021/acs.langmuir.6b04365.
48. Thijssen, J.H.J. and Vermant, J., *Interfacial Rheology of Model Particles at Liquid Interfaces and Its Relation to (Bicontinuous) Pickering Emulsions.* Journal of Physics: Condensed Matter, 2017. **30**(2): p. 023002 DOI: https://doi.org/10.1088/1361-648x/aa9c74.
49. Mason, T.G., Bibette, J. and Weitz, D.A., *Elasticity of Compressed Emulsions.* Physical Review Letters, 1995. **75**(10): p. 2051-2054 DOI: https://doi.org/10.1103/PhysRevLett.75.2051.
50. Mason, T.G., Bibette, J. and Weitz, D.A., *Yielding and Flow of Monodisperse Emulsions.* Journal of Colloid and Interface Science, 1996. **179**(2): p. 439-448 DOI: https://doi.org/10.1006/jcis.1996.0235.

51. Carrier, V. and Petekidis, G., *Nonlinear Rheology of Colloidal Glasses of Soft Thermosensitive Microgel Particles.* Journal of Rheology, 2009. **53**(2): p. 245-273 DOI: https://doi.org/10.1122/1.3045803.
52. Donley, G.J., Singh, P.K., Shetty, A. and Rogers, S.A., *Elucidating the G? Overshoot in Soft Materials with a Yield Transition Via a Time-Resolved Experimental Strain Decomposition.* Proceedings of the National Academy of Sciences of the United States of America, 2020. **117**(36): p. 21945-21952 DOI: https://doi.org/10.1073/pnas.2003869117.
53. Mason, T.G. and Weitz, D.A., *Linear Viscoelasticity of Colloidal Hard Sphere Suspensions near the Glass Transition.* Physical Review Letters, 1995. **75**(14): p. 2770-2773 DOI: https://doi.org/10.1103/PhysRevLett.75.2770.

SUPPORTING MATERIALS

Interfacial rheology of model water-air interfaces stabilized by microgels: effet of cross-linking.

Marie-Charlotte Tatry[1,2], Eric Laurichesse[1], Jan Vermant[3], Valérie Ravaine[2], Véronique Schmitt[1]

[1] Centre de Recherche Paul Pascal (CRPP), UMR 5031, Univ. Bordeaux, CNRS, 115 Avenue du Dr Albert Schweitzer, 33600 Pessac, FRANCE
[2] Univ. Bordeaux, CNRS, Bordeaux INP, ISM, UMR 5255, 33400 Talence, FRANCE
[3] Laboratory of Soft Materials, Department of Materials, ETH Zürich, Vladimir-Prelog-Weg 5, CH-8093, Zurich, SWITZERLAND

Supporting Information SI 1: details for the pNIPAM microgels synthesis

Polymerization was performed in a 500 mL three-neck round-bottom flask, equipped with a magnetic stir bar, a reflux condenser, thermometer, and argon inlet. NIPAM and the BIS cross-linker were dissolved in 280 mL of water so that the total monomer concentration was equal to 62 mM. The amount of BIS was varied from 1.5 to 5 mol% compared to NIPAM. The solutions were purified through a 0.2 mm membrane filter to remove residual particulate matter. The solutions were then heated up to 70°C with argon thoroughly bubbling during at least 1 h prior to initiation. Free radical polymerization was initiated with KPS (2.5 mM) dissolved in 20 mL of water after 10 min of argon degassing. The initially transparent solutions became progressively turbid as a consequence of the polymerization and precipitation processes. The solutions were allowed to react for a period of 6 h in the presence of argon under stirring. After this period of time, a homogeneous suspension was obtained.

Supporting Information SI 2: Scheme of the apparent dilational viscoelasticity measurement (left) and plot of E'_{app} versus π (right) using the pendant drop method. At a given time t, during adsorption that is to say at a given γ or equivalent at a given pressure π, oscillations were applied to measure E'_{app} and E''_{app}.

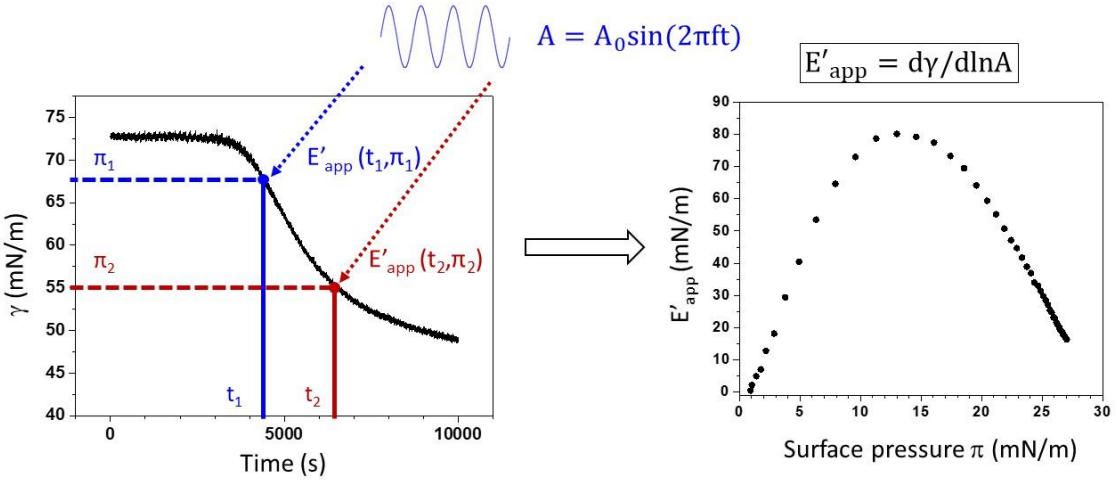

Supporting Information SI 3: Uniaxial compression elastic modulus as a function of the normalized area using Eq. 5 for the various microgels from table 1 (red disks: 1.5 mol%, blue diamonds: 2.5 mol% and black squares: 5 mol%)

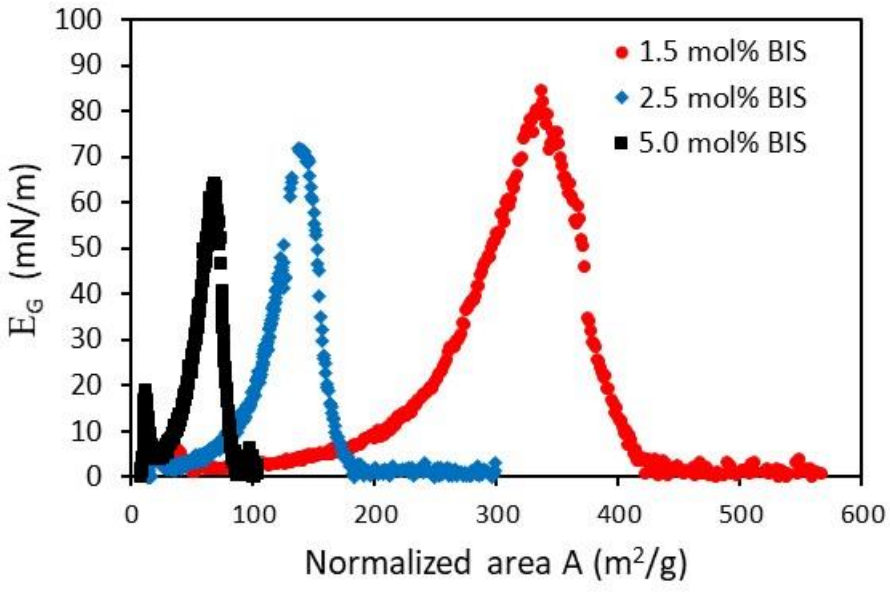

Supporting Information SI 4: Superposition of the curves given in Figure 5 for the various applied pressures. pNIPAM-1.5 laden air-water interface.

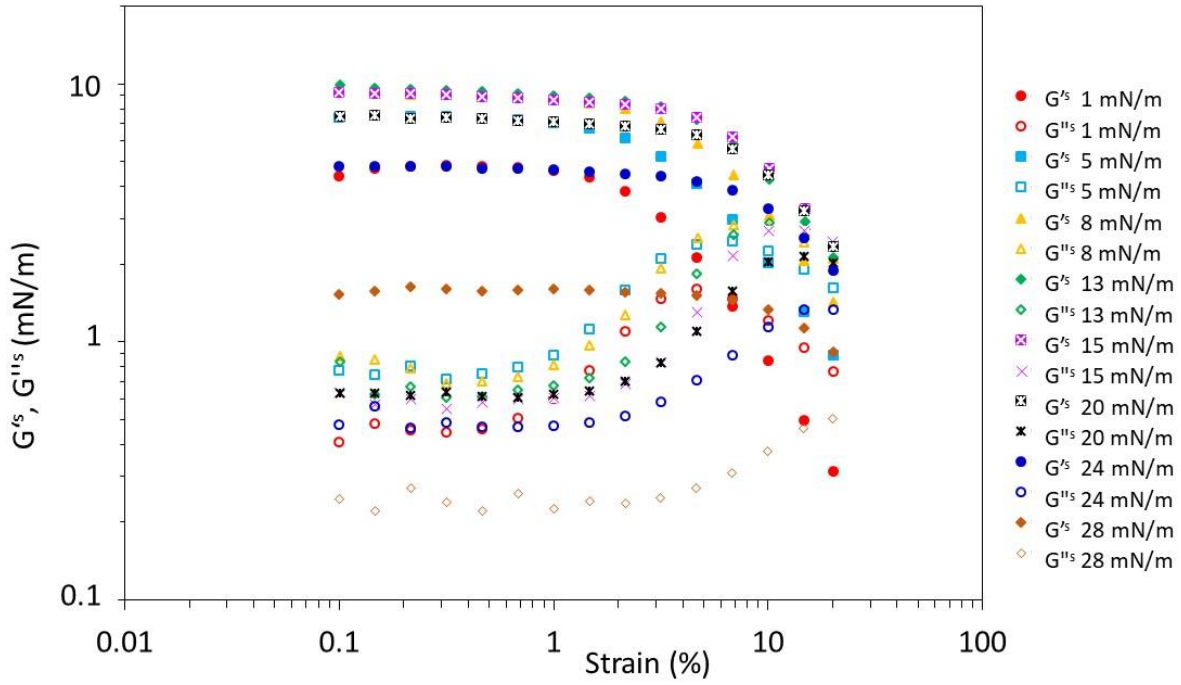

Supporting Information SI 5: Superposition of the curves given in Figure 6 for the various applied pressure. pNIPAM-5 laden air-water interface.

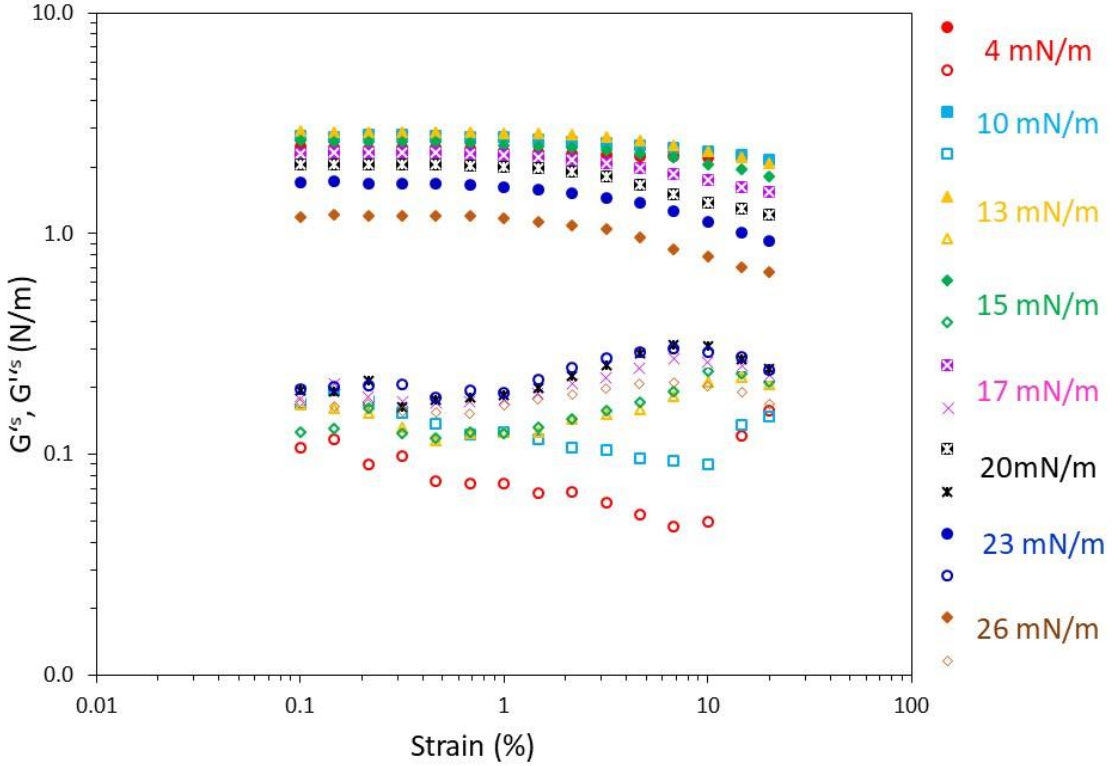

Supporting Information SI 6: examples of the determination of the surface critical values of the stress and strain oscillating amplitudes above which linearity is lost. They correspond to the limit of the VELD. Top: pNIPAM-1.5 with a 5 mN/m surface pressure, bottom: pNIPAM-5 with a 20 mN/m surface pressure.

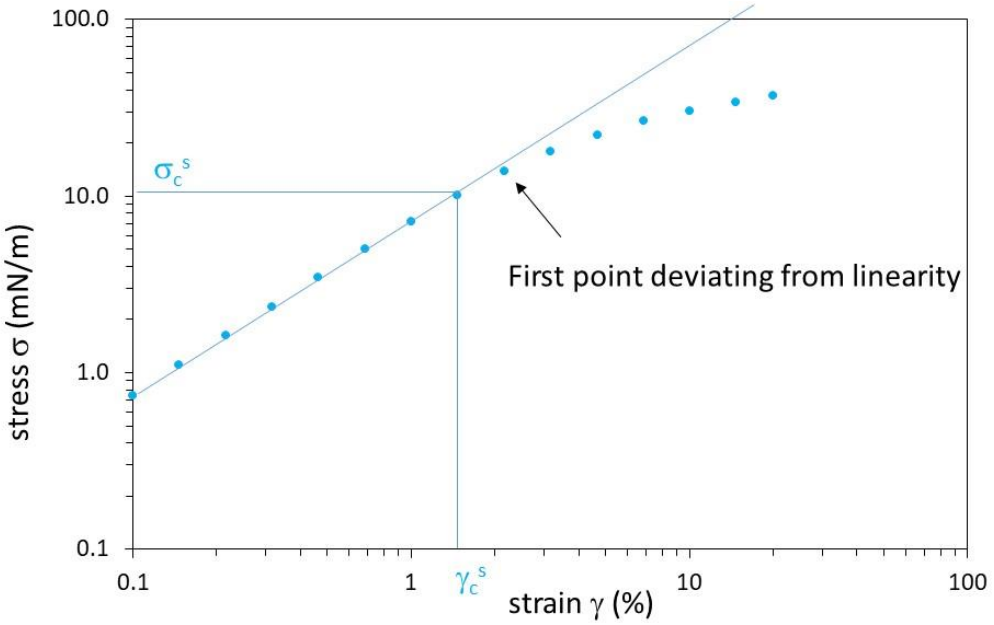

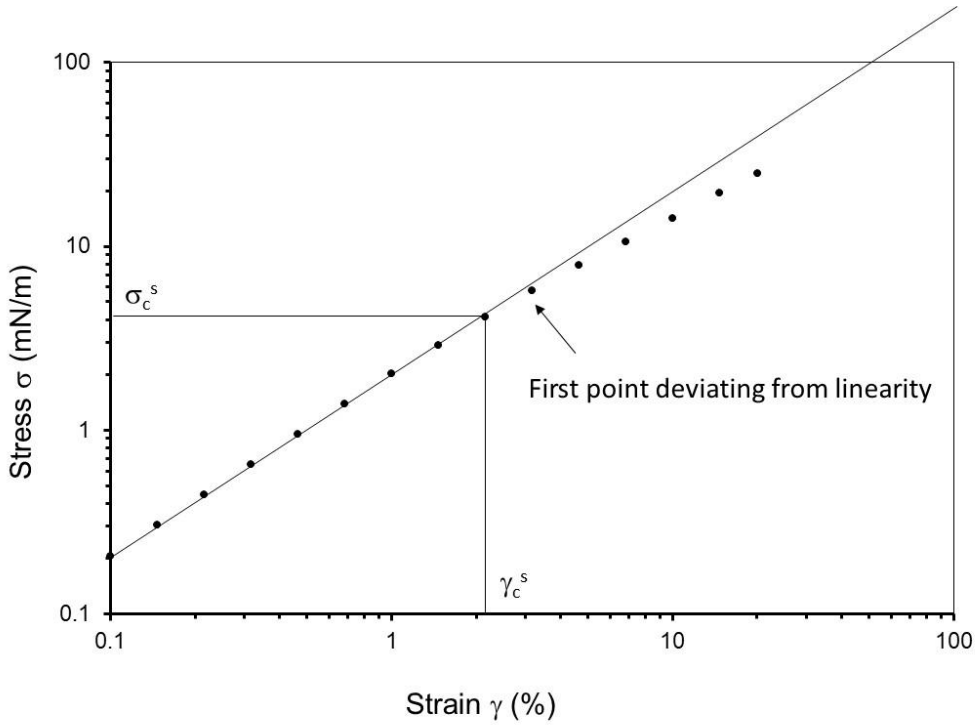

Supporting Information SI 7: Superposition of the curves given in Figure 10 for the pNIPAM-1.5 and pNIPAM-5.